Raman studies of vitreous SiO_2 versus fictive temperature

A. E. Geissberger and F. L. Galeener
Palo Alto Research Center, 3333 Coyote Hill Road, Palo Alto, California 94304
(Received 4 April 1983)

The first-order Raman spectra of vitreous SiO_2 have been studied as a function of sample fictive temperature T_F for $900\,°C \leq T_F \leq 1550\,°C$. Three observations were made: (1) The broad features assigned to vibrations associated with the continuous random network of v-SiO_2 shift in frequency in a manner consistent with densification by reduction of the average Si—O—Si angle θ; (2) the sharp "defect" lines at 492 and 606 cm^{-1} show little or no shift in frequency; (3) both defect line intensities exhibit Arrhenius behavior, $\exp(-\Delta E/k_B T_F)$, with well-defined activation energies ΔE of 0.14 and 0.40 eV, respectively. These observations are interpreted using a central-force network dynamics model and changes in the number of planar threefold and regular fourfold ring defects.

INTRODUCTION

Several physical properties of v-SiO_2 measured at room temperature are functions of the sample fictive temperature T_F (Ref. 1) (the fictive temperature is a higher temperature at which v-SiO_2 is allowed to reach an equilibrium state before a rapid quench to room temperature), so the network must undergo steric changes as a function of T_F. The aim of this paper is to relate the changes observed in the first-order Raman spectra to structural modifications of the v-SiO_2 network over the range $900 \leq T_F \leq 1550\,°C$. In particular, frequency shifts in the Raman spectra with increasing T_F are interpreted in terms of a slight decrease in the Si—O—Si bridging bond angle of v-SiO_2, according to a central-force network-dynamics model[2,3]; the increasing intensities of the two "defect" lines are interpreted as an increase in the number of regular ring defects in the glass, as previously proposed by Galeener.[4]

EXPERIMENTAL DETAILS

Materials preparation

Three different types of vitreous silica were used in this investigation. The majority of the measurements were made on General Electric type-214 clear fused-quartz GE214.[5] This is a very pure silica which has a nominal total metallic impurity concentration (TMI) of 50 ppm, 25 ppm of which is Al, and less than 1 ppm of any network-interrupting impurity such as Cl or OH. A few measurements were made on both Homosil,[6] which has a TMI less than 50 ppm, $\simeq$300 ppm OH, and Suprasil-1,[6] which has a TMI of less than 1 ppm and $\simeq$1200 ppm OH.[6] The GE214 samples were small beads, 3 mm in diameter, made by melting the end of a 2-mm glass rod in a hydrogen torch, and the Homosil and Suprasil-1 samples were rectangular parallelepipeds ($1\times5\times10$ mm^3).

In order to achieve the desired T_F the samples were heated at $T = T_F$ under flowing nitrogen to prevent devitrification by the action of water vapor. The samples were contained in 17×15 mm^2 open quartz tubes during the annealing. By placing the quartz vials inside an Al_2O_3 crucible and then inside a Pt crucible, the vertical loading elevator of the furnace could be dropped and the vials containing the samples plunged under water fast enough to reliably obtain $T_F = 1500\,°C$ samples from the GE214 material. To insure that the v-SiO_2 network had reached equilibrium at a given T_F, a series of Raman spectra were taken as a function of soaking time at T, and equilibrium was achieved when *all* measured frequencies and intensities were constant within experimental error. As observed in Ref. 7, the rates at which the samples approached equilibrium were functions of both T and the concentration of network-interrupting impurities (see below); however, the steady-state values of the measured frequencies and intensities were functions only of T_F.

Finally, samples were checked for any change in OH concentration as a result of heat treatment and quenching by measuring the 3700-cm^{-1} Raman-active OH stretch vibration.[8] Within the experimental error of $\leq 10\%$, there were no changes in the OH concentration of the samples in the sample region where the Raman spectra were measured.[9]

Raman spectroscopy

All Raman spectra were obtained in the 90° scattering configuration using 700 mW of power from the 457.9-nm line of an Ar laser. The beam was consistently focused on the center of a bead of GE214 fused silica or the same central region of the rectangular parallelepipeds of Homosil and Suprasil-1.

RESULTS AND DISCUSSION

Intensity variations with T_F

Figures 1(a) and 1(b) show typical Raman spectra obtained at $T_F = 1500$ and 1000 °C, respectively. The broad features are labeled ω_1, ω_3, ω_4(TO), and ω_4(LO) for reasons discussed in Ref. 3. They have been identified with vibrations of the glass network as described by a nearest-neighbor central-force dynamical theory[2,3] and are broad

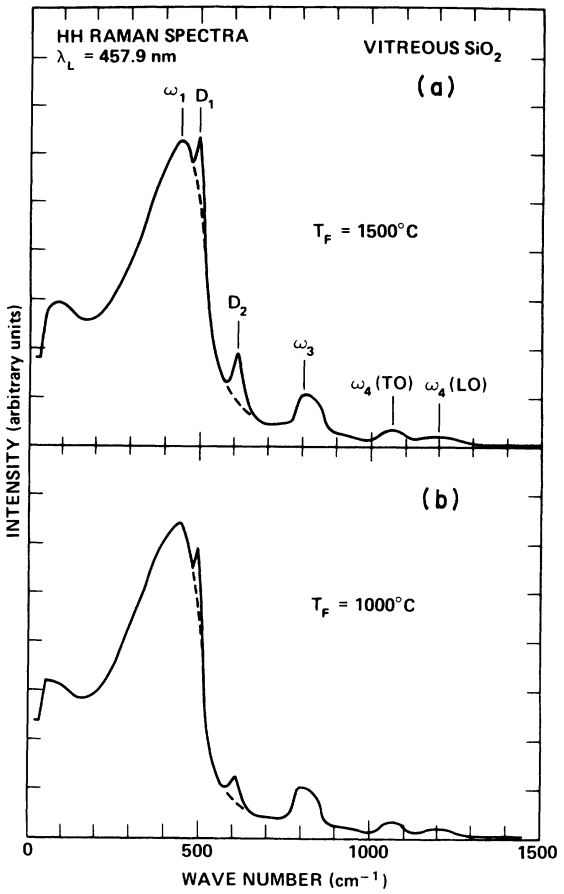

FIG. 1. Two *HH* Raman spectra [(a) $T_F = 1500$°C and (b) $T_F = 1000$°C] of v-SiO_2 showing the changes due to different fictive temperatures T_F. Features labeled ω_i have been identified with vibrations of the v-SiO_2 continuous random network, while features labeled D_i have been associated with regular ring defects. Dashed lines below the D_i features are typical baselines used in the area measurements given in Fig. 2.

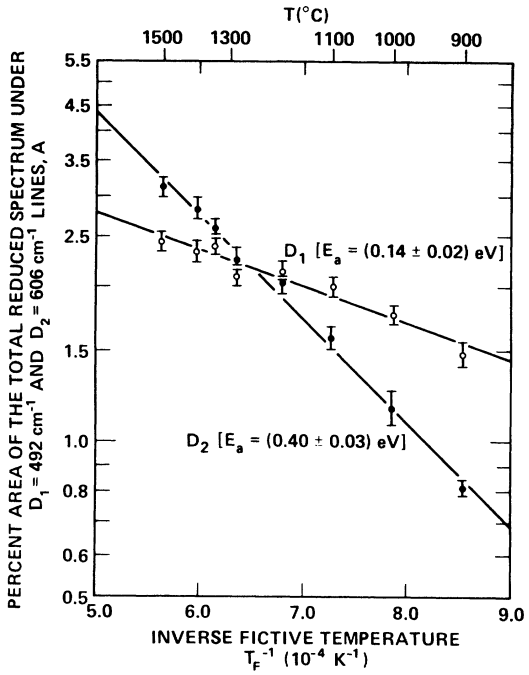

FIG. 2. Semilogarithmic plot of the percent area of the total reduced Raman spectrum under the D_1 (and D_2) relative maxima vs $1/T_F$. Points are the mean values of at least four area measurements taken at T_F and the length of an error bar equals two standard deviations of the area measurements at T_F. Straight lines are least-squares fits to the A_{D_1} and A_{D_2} data sets (see Table I).

because the Si—O—Si bond angles in that network are widely distributed. The so-called defect lines labeled D_1 and D_2 have been interpreted by Galeener[4] as arising from the symmetric stretch (SS) of regular fourfold and planar threefold rings embedded in the more irregular glass network that accounts for the broad lines. It is clear that the defect-line intensities increase with increasing T_F.

The defect-line intensities were measured by drawing a baseline, the dashed lines shown in Figs. 1(a) and 1(b), using a French curve, and the areas between the Raman spectra and the baseline were then measured gravimetrically. The actual spectra used in this procedure were taken with an expanded abscissa and care was taken to use the same section of the French curve to draw all baselines. This procedure was surprisingly accurate and gave highly reproducible results. The areas from different samples were then normalized against the peak height of the main line ω_1 at 440 cm^{-1}. (A check for a change in the relative intensity of the ω_3 and ω_4 network features to the ω_1-line peak height was made between 1100 and 1500°C: Within an experimental error of ±5%, there was no change.) Finally, the defect-line areas were converted into a percentage of the area of the total reduced first-order spectrum.

It has already been shown in Ref. 7 that the area under D_2 changes exponentially with $1/T_F$, so our data are shown in Fig. 2 as a semilogarithmic plot of area versus $1/T_F$. The points are mean values obtained from at least four spectra and each error bar represents two standard deviations of the measurements of the defect line area at T_F. The straight lines for D_1 and D_2, which are least-squares fits to the data, demonstrate that *both* defect-line intensities exhibit Arrhenius behavior, $\exp(-\Delta E/k_B T_F)$.

The regression coefficients of the lines in Fig. 2 are given in Table I along with the correlation coefficients and 99% confidence intervals[10] for the D_1 and D_2 energies of formation, $E_a = 0.14 \pm 0.02$ and 0.40 ± 0.03 eV, respectively. The E_a for D_2 is in good agreement with the value (0.44 eV) obtained previously by Mikkelsen and Galeener.[7] Similar values were predicted by Galeener[4] for ring defects using energies derived from an *ab initio* self-consistent-field molecular-orbital (SCF-MO) calculation of Newton and Gibbs.[11] In particular, Galeener estimated a formation energy of 0.16 eV for fourfold planar ring defects and 0.51 eV for threefold planar ring defects, and he assigned the D_1 and D_2 lines to the SS vibration of four- and threefold rings, respectively. The agreement between the present empirical "activation" energies and the predicted

TABLE I. Regression-analysis parameters of the semilogarithmic fits to the A_{D_1} and A_{D_2} data sets shown in Fig. 2. E_a tolerances were obtained from 0.99% confidence intervals for the slopes of the least-squares-fit lines. These confidence intervals were calculated under the assumptions of normal regression analysis using the t distribution (Ref. 10).

Data set	Number of points	Intercept	Slope	Correlation coefficient	99% confidence interval for E_a (eV)
A_{D_1}	44	6.23	−0.160	−0.940	0.14±0.02
A_{D_2}	40	44.2	−0.462	−0.989	0.40±0.03

values supports the assignment of the D_1 and D_2 defect lines to regular (possibly puckered) fourfold and planar threefold ring structures in v-SiO_2.

Frequency variations with T_F

Table II and Fig. 3 show the measured frequencies of the v-SiO_2 Raman spectral features as a function of T_F. These frequencies were obtained using expanded scales and by carefully bisecting the features in order to project the peak position onto the frequency axis. The error in all frequency measurements is estimated to be ± 1.5 cm^{-1}. The straight lines shown in Fig. 3 are least-squares fits to the data. We do not expect the Raman frequencies to be exactly linear functions of T_F, but an *approximately* linear dependence of ω_i on T_F is implied by the "scattergram" shown in Fig. 3. The parameters in columns 4 and 5 of Table III indicate that a straight line provides a good fit to the ω_i-vs-T_F data. On the basis of the ring model, however, we expect the D_i frequencies to show little or no correlation with T_F; this is because the ring geometries are basically fixed as are, therefore, their SS frequencies. The slopes of the D_1 and D_2 lines in Fig. 3 indicate less change than for the network features and the fit parameters in columns 4 and 5 show that there may be no dependence of their frequencies on T_F. Thus there are qualitative differences in the variation of the ω_i and D_i lines with T_F: The ω_i lines show little or no relative intensity variation but definite frequency shifts, while the D_i lines show large intensity changes with little or no frequency shifts.

The ω_i frequencies are predicted to be dependent upon the Si—O—Si bridging bond angle θ by a central-force idealized continuous-random-network (CF-ICRN) theory.[2,3] Their frequencies are given by the equations

$$\omega_1^2=(\alpha/m_O)(1+\cos\theta)\ , \tag{1}$$

$$\omega_3^2=(\alpha/m_O)(1+\cos\theta)+(4\alpha/3m_{Si})\ , \tag{2}$$

$$\omega_4^2=(\alpha/m_O)(1-\cos\theta)+(4\alpha/3m_{Si})\ . \tag{3}$$

Here, ω_i are the angular frequencies (in rad/sec) while m_O and m_{Si} are the masses of the oxygen and silicon atoms and α is the Si—O bond-stretching force constant. (All other force constants are assumed to be zero.) For small changes in θ, we can relate $\Delta\theta$ to $\Delta\omega_i$ by differentiating Eqs. (1)—(3) to obtain

$$\Delta\omega_i=\pm(\alpha/m_O)\sin\theta\,\Delta\theta/2\omega_i\ , \tag{4}$$

where the sign is negative for $i=1$ and 3 and positive for $i=4$. Equations (1)—(4) elucidate the changes in ω_i with T_F, in particular the opposite signs of the $\omega_{1,3}$ and ω_4 shifts: Densification of the network with increasing T_F occurs by reducing the average value of θ,[12,13] and therefore $\Delta\theta$ in Eq. (4) is negative and $\Delta\omega_i$ is positive for ω_1 and ω_3 and negative for ω_4. Here, as before,[3] we use

TABLE II. Frequencies of the relative maxima of the first-order v-SiO_2 Raman spectra as a function of fictive temperature T_F. Some of the ω_i values are the average of two runs plotted in Fig. 3. All of these peak positions were taken with the incident beam polarized parallel to the scattered light (HH) except for ω_3, which was measured with the scattered-light electric field vector perpendicular to the incident-beam electric field vector (HV).

T_F (°C)	ω_1 (cm^{-1})	ω_3 (cm^{-1})	ω_4(TO) (cm^{-1})	ω_4(LO) (cm^{-1})	D_1 (cm^{-1})	D_2 (cm^{-1})
900	435	791	1067	1199	490	605
1000	437.5	792	1066	1196.5	491	606.5
1100	437.5	793	1064	1193	490.5	606
1200	440	793	1062	1192.5	490.5	605.5
1300	442	793	1061	1188	492	605
1400	443	794	1058	1188	492.5	606
1500	445.5	794	1058	1188	492.5	606
1550[a]	448	795	1056	1187	493.5	607.5
4000[b]	460	805	1038	1175	500	608

[a] Sample water quenched from white heat; T_F calculated from D_2 area.

[b] Neutron-irradiated sample (2×10^{20} n/cm^{-2}); Raman data from Ref. 15; T_F calculated from D_2 area.

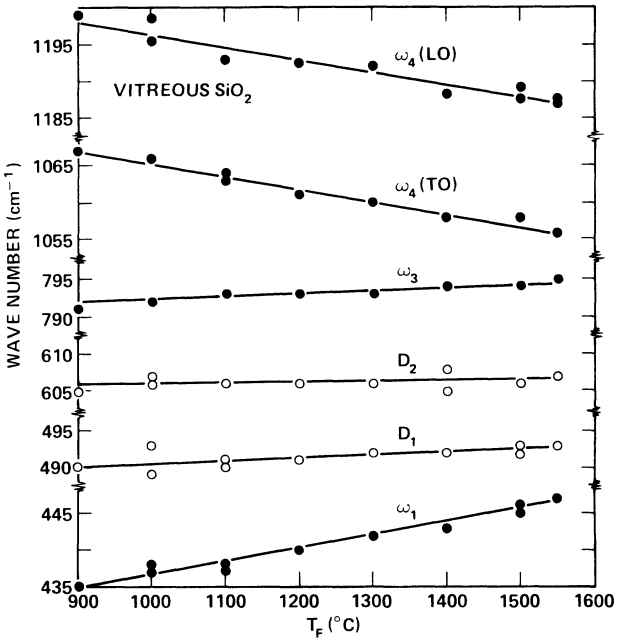

FIG. 3. Plot of the peak positions of the Raman features as a function of T_F. Note that the values of ω_1 and ω_3 increase with increasing T_F while those of ω_4 decrease, as predicted by the CF theory associated with Eqs. (1)–(4). Lines drawn through the points are least-squares fits to the data and the parameters of the fits are given in Table III.

$\alpha=545$ N/m and $\theta=130°$. Column 3 of Table IV shows the results of applying these equations to the total frequency shifts observed between $T_F=900$ and 1550°C. Since the CF-ICRN theory is known to be approximate,[3] we are not surprised that each ω_i returns a somewhat different value of $\Delta\theta$. The average value of $\Delta\theta$, $-2.0°$, is consistent with x-ray data on thermally compacted v-SiO_2,[13] and the CF-ICRN theory also yields the correct angle change for radiation-compacted v-SiO_2 (see below). The correct sign predictions and reasonable values of $\Delta\theta$ given by the CF theory support the general validity of this approach to the study of network dynamics in the vitreous state and should encourage further refinement of the theory to include the effects of noncentral forces.

We make two final statements with regard to the defect-line frequency behavior. First, most of the correlation of the D_1 defect line with T_F may be due to its proximity to the much stronger main line, ω_1; therefore, D_1 may be entirely independent of T_F. Second, the D_1 *and* D_2 frequencies have been found to be independent of Si atomic mass, as demonstrated by isotopic substitution experiments.[14] The stability of these frequencies is consistent with their assignment to the SS of regular ring defects.

Relaxation times versus T_F

While obtaining the above data we made several measurements of certain relaxation times associated with the D_1, D_2, and ω_1 lines. For D_1 and D_2 we anneal the sample to equilibrium defect-line strength at an elevated temperature T_0, then quench to room temperature and measure the area A_0 under the line in question. Next the temperature is raised abruptly to an "annealing" temperature T_A, a few hundred °C below T_0. After a time t^* the sample is again quenched to room temperature and $A(t^*)\equiv A^*$ is measured. Finally, the sample is abruptly raised to T_A and kept there until a steady-state area A_∞ is achieved, corresponding to a practical value of $t\rightarrow\infty$. Several points are obtained in preliminary runs, so that the times necessary for achieving A_0 and A_∞ are known, and so that t^* can be chosen such that the intermediate change in area $[A^*-A_\infty]$ has a convenient value. We then assume that the data are fit by an exponential decay in time according to

$$A(t)-A_\infty=[A_0-A_\infty]e^{-t/\tau}\,, \tag{5}$$

and compute τ using the measured A_0, A^*, t^*, and A_∞,

$$\tau=t^*/\ln[(A_0-A_\infty)/(A^*-A_\infty)]\,. \tag{6}$$

As pointed out in Ref. 7, the data are not represented exactly by Eq. (5), so we have in effect fit only to three specially chosen data points (at $t=0$, t^*, and ∞). Nevertheless the effective relaxation times τ determined by this procedure give, with the use of Eq. (5), a useful representa-

TABLE III. Regression-analysis parameters of the wave-number–vs–T_F data sets shown in Table II. 95% confidence intervals for the slopes were calculated under the assumptions of normal regression analysis using the t distribution (Ref. 10).

1 Data set	2 Intercept (cm^{-1})	3 Slope (10^{-3} cm^{-1}/°C)	4 95% confidence interval for slope (10^{-3} cm^{-1}/°C)	5 Correlation coefficient
ω_1	418	18	±3.4	0.983
ω_3	787	5.1	±1.6	0.953
ω_4(TO)	1082	−17	±2.3	−0.991
ω_4(LO)	1214	−18	±5.6	−0.956
D_1	486	4.9	±5.0	0.922
D_2	604	1.7	±3.0	0.479

TABLE IV. Total change in the bridging oxygen bond angle θ predicted by Eqs. (1)—(4) for heat-treated and neutron-irradiated v-SiO_2. Total changes in wave number for the heat-treated and neutron-irradiated v-SiO_2 were calculated from measurements on $T_F=900$ and 1550 °C samples, and unirradiated and 2×10^{20} n/cm^2 irradiated material, respectively.

1	Heat-treated v-SiO_2 (ΔT_F: 900→1550 °C)		Neutron-irradiated v-SiO_2 (unirradiated vs 2×10^{20} n/cm^2)	
Network	2	3	4	5
feature	$\Delta\omega_{total}$ (cm^{-1})	$\Delta\theta$ (deg)	$\Delta\omega_{total}$ [a] (cm^{-1})	$\Delta\theta$ (deg)
ω_1	13	−1.5	25	−2.9
ω_3	4	−0.83	12	−2.5
ω_4(TO,LO)	−12	−3.7	−25	−7.8

[a] Raman data from Ref. 15.

tion of the time decay of defect concentration. The T_0, T_A, t^*, and τ values for several samples and situations are given in Table V.

We make two observations with regard to this data. First, the relaxation times for both defect lines are functions of T_A and the level of network-terminating impurities (e.g., OH content), as reported previously[7] for the D_2 relaxation time. Second, the average value of τ_1/τ_2 is 1.9. Since E_a for D_1 is less than that of D_2, this is rather surprising; however, if D_1 and D_2 are indeed due to the SS of four- and threefold ring defects, the observed ratio can be understood in terms of greater steric hindrances of the network towards the construction of a fourfold ring over a threefold ring.

In addition to measuring the aforementioned effective relaxation times for the D_i intensities, we made one measurement of the thermally induced relaxation time for the *frequency* ω_1 in GE214. This was done using the same procedure as above, with the frequency relaxation time computed according to

$$\tau_{\omega 1}=t^*/\ln[(\omega_0-\omega_\infty)/(\omega^*-\omega_\infty)]\ . \tag{7}$$

For $T_0=1400$ °C, $T_A=1100$ °C, $t^*=7.2\times10^3$ sec, and $\tau_{\omega 1}=3.3\times10^3$ sec. Thus, τ_{ω_1} is approximately $\frac{1}{10}$ of the defect-intensity relaxation time for a similar heat treatment (see Table V). This observation also seems consistent with the assignment of D_1 and D_2 to ring defects and ω_1 to the SS of the network-bridging oxygen atoms. It would seem to be easier and quicker to adjust the network angles θ to a slightly smaller value than to "restructure" bonds and produce a smaller number of regular rings.

Variations in the Raman spectrum versus neutron irradiation

Finally, we consider the changes in the Raman spectra of neutron-irradiated v-SiO_2 observed by Bates, Hendrick, and Shaffer[15] (BHS) in light of the above analysis. The changes in the defect lines reported by BHS as a function of neutron irradiation were similar to those we have ob-

TABLE V. Characteristic relaxation times τ_i for the D_1 and D_2 concentrations as measured by the corresponding line intensities $A(t)$. Here T_0 is the initial equilibration temperature of the sample, T_A is the annealing temperature, and t^* is the time the sample was held at T_A in order to enable calculation of τ from Eq. (5). [GE214 is General Electric type-214 clear fused quartz (Ref. 5).]

Sample material	T_0 (°C×10^2)	T_A (°C×10^2)	t^* (sec)	τ_1 (sec)	τ_2 (sec)	τ_1/τ_2
Suprasil-1	13	9.0	5.4×10^3	4.8×10^3	4.5×10^3	1.1
Suprasil-1	13	11	1×10^2	6.8×10^1	4.3×10^1	1.6
Homosil	13	11	7.6×10^3	1.2×10^4	7.0×10^3	1.7
Homosil	13	11	1.4×10^4	1.1×10^4	9.1×10^3	1.2
GE214	13	11	7.6×10^3		2.2×10^4	
GE214	13	11	2.3×10^4	6.3×10^4	6.1×10^4	1.0
GE214	13	11	3.7×10^4	2.2×10^5	3.6×10^4	6.1
GE214	14	11	2.3×10^4	4.2×10^4	2.1×10^4	2.0
GE214	14	11	4.7×10^4	3.5×10^4	3.5×10^4	1.0
GE214	14.5	11	2.3×10^4	3.3×10^4	1.6×10^4	2.1
GE214	14.5	11	5.0×10^4	3.4×10^4	3.2×10^4	1.1
GE214	14	12	1.5×10^3	2.8×10^3	1.4×10^3	2.0
GE214	14	12	1.8×10^3	1.3×10^3	9.3×10^2	1.4

served as a function of T_F, except they were of greater magnitude. In an extensive discussion of other properties of D_1 and D_2, Galeener[16] has speculated that their high concentration in neutron-irradiated v-SiO_2 might be explained by a very high T_F associated with the "thermal-spike" model of neutron damage. In Table III of Ref. 15, BHS report an increase in the intensity of the D_2 line by a factor of 7.3 after exposure to 2×10^{20} n/cm^2. Extrapolating our Arrhenius plot of D_2, we predict the T_F of this sample to be $T_F^*\simeq4000$ K, assuming the unirradiated sample had a D_2 line intensity before irradiation characteristic of a sample with $T_F=1213$ °C, the annealing point of General Electric fused quartz.[5] (Our as-delivered GE214 had a D_2 intensity characteristic of a sample with $T_F=1180$ °C.) This is in reasonable agreement with the local temperature T_L defined by Primak, Edwards, Keifer, and Szymanski,[17] who describe neutron-irradiation changes in v-SiO_2 as a collection of highly localized phase changes, each characterized by extreme local conditions of temperature (thermal spike) and pressure around the site of the primary knocked-on atom. They estimated the affected volume to be 10^4 atoms, the local temperature to be 5000–10 000 °C and a local pressure of 3000–7000 atm. This extremely small volume would allow a rapid quench rate in the impact volume, and so a very high T_F could be achieved for the entire sample provided it was exposed to sufficient neutron flux such that every microscopic volume of the sample was "melted." If not, the Raman spectrum would be a weighted average of the spectrum for the local fictive temperature T_L and the original fictive temperature T_0. (We note that the fraction of unmelted fictive-temperature material is probably small but not zero for a flux of 2×10^{20} n/cm^{-2}; see Fig. 5 in Ref. 15.) The Raman spectrum of neutron-irradiated v-SiO_2, therefore, should change in a continuous manner as more material undergoes the gradual, rapidly quenched vitrification. With the use of the ICRN equations for $\omega_i(\theta)$, we calculated the results shown in column 5 of Table IV from the changes in ω_i between the unirradiated and the 2×10^{20}-n/cm^{-2} BHS samples. The average $\Delta\theta$, $-4.4°$, is in good agreement with the value $-4°$ obtained by x-ray-diffraction spectroscopy of neutron-irradiated v-SiO_2.[18]

SUMMARY

We have investigated the changes in the Raman spectrum as a function of fictive temperature T_F and related them to steric modifications of the v-SiO_2 network. For $900\le T_F\le1500$ °C we observed modest shifts in the frequencies of the host-network vibrational modes and strong changes in the intensity of the two defect modes (with little or no change of their frequencies). The shift of the network mode frequencies were related to a 2.0° reduction in the Si—O—Si bridging bond angle θ with increasing T_F. The intensity changes in both the 492-cm^{-1} D_1 and 606-cm^{-1} D_2 defect modes were shown to exhibit Arrhenius behavior with activation energies of 0.14 ± 0.02 and 0.40 ± 0.03 eV, respectively. These activation energies are taken as strong support for Galeener's earlier assignment[4] of the D_1 and D_2 modes to regular fourfold and planar threefold ring defects. The changes in the intensities of D_1 and D_2 were shown to have different characteristic relaxation times with $\tau_1/\tau_2=1.9$ on the average. All of the changes in the Raman spectrum due to increasing the sample T_F, as well as those due to increasing neutron irradiation, can be understood in terms of a slight reduction in the average Si—O—Si bridging bond angle θ and an increase in the number of regular ring defects.

ACKNOWLEDGMENTS

The authors are grateful to the U. S. Navy Office of Naval Research (G. B. Wright) for support of this work under Contract No. N00014-80-C-0713.

[1]R. Bruckner, J. Non-Cryst. Solids 5, 123 (1970).
[2]P. N. Sen and M. F. Thorpe, Phys. Rev. B 15, 4030 (1977).
[3]F. L. Galeener, Phys. Rev. B 19, 4292 (1979).
[4]F. L. Galeener, J. Non-Cryst. Solids 49, 53 (1982); Solid State Commun. 44, 1037 (1982).
[5]Product Data Sheet 7710-f, General Electric Company, General Electric Company, Quartz and Chemical Products Dept., 24400 Highland Rd., Richmond Heights, OH 44143 [December (1977)].
[6]Amersil Inc., Fairfield, NJ; W. Primak, in *The Compacted States of Vitreous Silica* (Gordon and Breach, New York, 1975).
[7]J. C. Mikkelsen, Jr. and F. L. Galeener, J. Non-Cryst. Solids 37, 71 (1980).
[8]F. L. Galeener and R. H. Geils, in *The Structure of Non-Crystalline Materials*, edited by P. H. Gaskell (Taylor and Francis, London, 1977), p. 223.
[9]F. L. Galeener and J. C. Mikkelsen, Jr., Appl. Phys. Lett. 38, 336 (1981).
[10]See, for example, J. E. Freund, *Mathematical Statistics*, 2nd ed. (Prentice-Hall, Englewood Cliffs, New Jersey, 1971), p. 386.
[11]M. D. Newton and G. V. Gibbs, Phys. Chem. Minerals 6, 221 (1980).
[12]W. Primak, *The Compacted States of Vitreous Silica* (Gordon and Breach, New York, 1975), p. 26.
[13]V. E. Sokol'skii, V. A. Shovskii, V. P. Kazimirov, and G. I. Batalin, Sov. J. Glass Phys. Chem. (USA) 6, 338 (1980).
[14]F. L. Galeener and A. E. Geissberger, Phys. Rev. B 27, 6199 (1983).
[15]J. B. Bates, R. W. Hendricks, and L. B. Shaffer, J. Chem. Phys. 61, 4153 (1974).
[16]F. L. Galeener, in *The Structure of Non-Crystalline Materials II*, edited by P. H. Gaskell, A. E. Davis, and J. N. Parker (Taylor and Francis, London, 1983), p. 337.
[17]W. Primak, E. Edwards, D. Keifer, and H. Szymanski, Phys. Rev. 133, A531 (1964).
[18]I. Simon, J. Am. Ceram. Soc. 40, 150 (1957).